



Synthesis, crystal structure and thermal decomposition pathway of bis(isoselenocyanato- κ N)tetrakis(pyridine- κ N)manganese(II)

Christian Näther,* Sebastian Mangelsen and Jan Boeckmann

Institut für Anorganische Chemie, Universität Kiel, Max-Eyth-Strasse 2, 24118 Kiel, Germany. *Correspondence e-mail: cnaether@ac.uni-kiel.de

Received 14 April 2023

Accepted 18 April 2023

Edited by W. T. A. Harrison, University of Aberdeen, United Kingdom

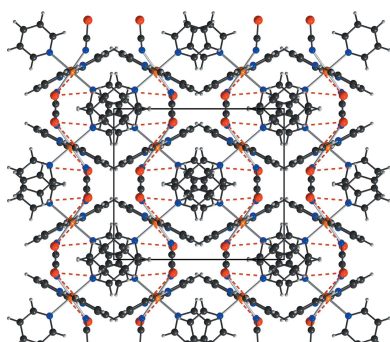
Keywords: crystal structure; nickel selenocyanate; discrete complex; thermal properties.**CCDC reference:** 2257160**Supporting information:** this article has supporting information at journals.iucr.org/e

The reaction of $\text{MnCl}_2 \cdot 2\text{H}_2\text{O}$ with KSeCN and pyridine in water leads to the formation of the title complex, $[\text{Mn}(\text{NCSe})_2(\text{C}_5\text{H}_5\text{N})_4]$, which is isotypic to its Fe, Co, Ni, Zn and Cd analogues. In its crystal structure, discrete complexes are observed that are located on centres of inversion. The Mn cations are octahedrally coordinated by four pyridine coligands and two selenocyanate anions that coordinate *via* the N atom to the metal centres to generate *trans*- $\text{MnN}(s)_2\text{N}(p)_4$ octahedra (s = selenocyanate and p = pyridine). In the extended structure, weak $\text{C}-\text{H} \cdots \text{Se}$ contacts are observed. Powder X-ray diffraction (PXRD) investigations prove that a pure sample was obtained and in the IR and Raman spectra, the C–N stretching vibrations are observed at 2058 and 2060 cm^{-1} , respectively, in agreement with the terminal coordination of the selenocyanate anions. Thermogravimetric investigations reveal that the pyridine coligands are removed in two separate steps. In the first mass loss, a compound with the composition $\text{Mn}(\text{NCSe})_2(\text{C}_5\text{H}_5\text{N})_2$ is formed, whereas in the second mass loss, the remaining pyridine ligands are removed, which is superimposed with the decomposition of $\text{Mn}(\text{NCSe})_2$ formed after ligand removal. In the intermediate compound $\text{Mn}(\text{NCSe})_2(\text{C}_5\text{H}_5\text{N})_2$, the CN stretching vibration is observed at 2090 cm^{-1} in the Raman and at 2099 cm^{-1} in the IR spectra, indicating that the Mn cations are linked by μ -1,3-bridging anionic ligands. PXRD measurements show that a compound has formed that is of poor crystallinity. A comparison of the powder pattern with that calculated for the previously reported $\text{Cd}(\text{NCSe})_2(\text{C}_5\text{H}_5\text{N})_2$ indicates that these compounds are isotypic, which was proven by a Pawley fit.

1. Chemical context

Coordination compounds based on transition-metal thio- and selenocyanates can be divided into two major groups. In the first group, the anionic ligands are only terminally coordinated, which leads with monocoordinating ligands to discrete complexes that are of interest, for example, in the field of spin-crossover materials (Gütlich *et al.*, 2000; Senthil Kumar & Ruben, 2017). In the second group, the anionic ligands act as bridging ligands, which is of structural interest, because a variety of structures with one-, two- or three-dimensional networks can form. Moreover, because these ligands can mediate magnetic exchange, they are also of interest in the field of molecular magnetism (Shurdha *et al.*, 2013; Palion-Gazda *et al.*, 2015; Prananto *et al.*, 2017; Mekuimemba *et al.*, 2018). In this context, compounds based on Co^{II} cations are of special interest because of the strong magnetic anisotropy (Werner *et al.*, 2014; Rams *et al.*, 2020*a,b*; Mautner *et al.*, 2018).

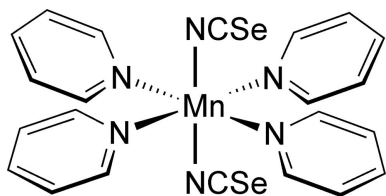
In the majority of cases, the synthesis of thio- and selenocyanate coordination compounds is performed in solution, that with less chalcophilic metal cations frequently leads to the



OPEN ACCESS

Published under a CC BY 4.0 licence

formation of compounds with terminal anionic ligands. In contrast, the synthesis of compounds with a bridging coordination is more difficult to achieve, even if an excess of the metal salt is used in the synthesis. This behaviour is even more pronounced for selenocyanate compounds. In such cases, an alternative approach was developed, in which precursor complexes with terminal thio- or selenocyanate anions are thermally decomposed, leading to the removal of the coligands in separate steps (Wriedt & Näther, 2010; Wöhlert *et al.*, 2012). In the course of this irreversible reaction, the desired compounds with bridging anionic ligands are obtained in quantitative yields. This approach is of special interest for the synthesis of selenocyanate coordination polymers because, on one hand, they are frequently difficult to prepare and, on the other hand, only a few such compounds with paramagnetic metal cations are reported in the literature. This method, however, can always be successfully applied for the synthesis of thiocyanates, whereas for selenocyanates sometimes the thermogravimetric (TG) curves are poorly resolved and in some cases poorly crystalline or even amorphous residues are obtained; the reason for this behavior is unknown (Wriedt & Näther, 2010).



This is the case, for example, for compounds with the composition $M(\text{NCSe})_2(\text{C}_5\text{H}_5\text{N})_2$, with $M = \text{Fe}$, Co or Ni ($\text{C}_5\text{H}_5\text{N}$ is pyridine). The Fe and Co compounds are isotypic to their thiocyanate analogs and consist of octahedrally coordinated metal cations that are linked by pairs of μ -1,3-bridging anionic ligands into chains (Boeckmann & Näther, 2011; Boeckmann *et al.*, 2012). None of these compounds can be

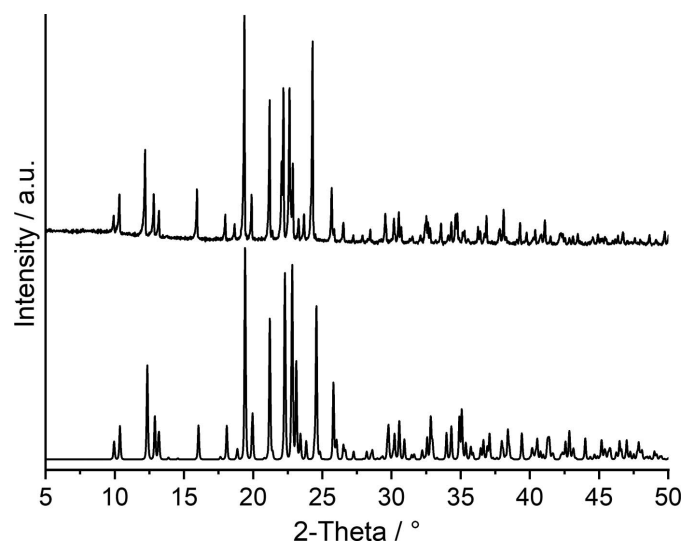


Figure 1
Experimental (top) and calculated PXRd patterns (bottom) of the title compound.

Table 1
Selected geometric parameters (\AA , $^\circ$).

Mn1–N1	2.196 (3)	Mn1–N21	2.317 (3)
Mn1–N11	2.307 (3)		
N1–Mn1–N11 ⁱ	90.59 (10)	N11–Mn1–N21	92.03 (9)
N1–Mn1–N11	89.41 (10)	N11–Mn1–N21 ⁱ	87.97 (9)
N1 ⁱ –Mn1–N21	90.02 (10)	N1–C1–Se1	179.1 (3)
N1–Mn1–N21	89.98 (10)	C1–N1–Mn1	151.4 (3)

Symmetry code: (i) $-x + \frac{3}{2}, -y + \frac{3}{2}, -z + 1$.

prepared from solution but the Fe compound is obtained as a pure crystalline material by thermal decomposition of its precursor, whereas the residue obtained for Co is amorphous. However, the Co compound can be prepared in crystalline form by thermal annealing below the decomposition temperature obtained from TG measurements (Boeckmann & Näther, 2011). The Ni compound is also available by thermogravimetry, even if it is of low crystallinity, but comparison of the experimental powder X-ray diffraction (PXRd) pattern obtained after the first mass loss shows that $\text{Ni}(\text{NCSe})_2(\text{C}_5\text{H}_5\text{N})_2$ is not isotypic to $M(\text{NCSe})_2(\text{C}_5\text{H}_5\text{N})_2$, with $M = \text{Fe}$, Co and Cd (Näther & Boeckmann, 2023). Its crystal structure is still unknown and in this context it is mentioned that the occurrence of different modifications, including polymorphs or isomers, is frequently observed for such thiocyanate coordination compounds (Werner *et al.*, 2015). However, in this case, the question arose if the Mn compound is also available as a crystalline material and if it will adopt the structure type of its Fe, Co and Cd analogs or that of $\text{Ni}(\text{NCSe})_2(\text{C}_5\text{H}_5\text{N})_2$.

To answer this question, much effort was made to synthesize the desired compound $\text{Mn}(\text{NCSe})_2(\text{C}_5\text{H}_5\text{N})_2$ in solution, but the pyridine-rich title compound $\text{Mn}(\text{NCSe})_2(\text{C}_5\text{H}_5\text{N})_4$ was always obtained. Single-crystal X-ray diffraction proved that it

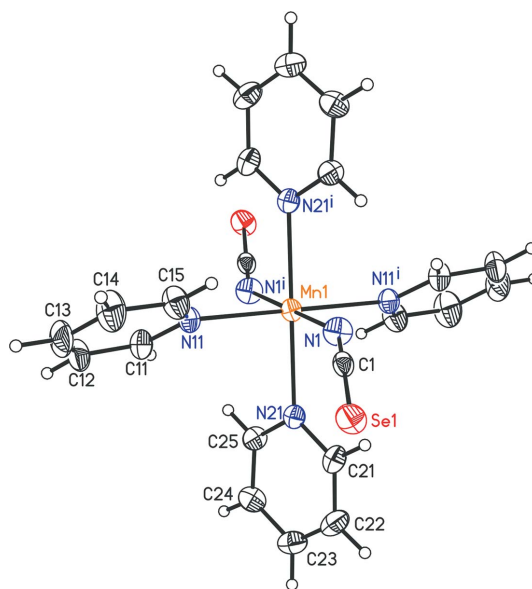


Figure 2
The crystal structure of the title compound, showing the atom labelling and with displacement ellipsoids drawn at the 50% probability level. [Symmetry code: (i) $-x + \frac{3}{2}, -y + \frac{3}{2}, -z + 1$.]

Table 2
Hydrogen-bond geometry (Å, °).

$D-H\cdots A$	$D-H$	$H\cdots A$	$D\cdots A$	$D-H\cdots A$
C12–H12 \cdots Se1 ⁱⁱ	0.95	3.10	3.992 (4)	156
C22–H22 \cdots Se1 ⁱⁱⁱ	0.95	3.11	3.986 (4)	155
C25–H25 \cdots Se1 ^{iv}	0.95	3.04	3.757 (3)	133
C25–H25 \cdots N1 ⁱ	0.95	2.65	3.247 (4)	121

Symmetry codes: (i) $-x + \frac{3}{2}, -y + \frac{3}{2}, -z + 1$; (ii) $-x + 1, -y + 1, -z + 1$; (iii) $-x + 1, y, -z + \frac{3}{2}$; (iv) $x + \frac{1}{2}, y - \frac{1}{2}, z$.

is isotopic to its Cd, Zn, Fe, Co and Ni analogs (Boeckmann *et al.*, 2011, 2012; Boeckmann & Näther, 2011; Näther & Boeckmann, 2023) and comparison of the experimental PXRD pattern with that calculated from the single-crystal data proves that a pure phase was obtained (Fig. 1). Therefore, this compound was used as a precursor for TG investigations to check if the pyridine-deficient compound $Mn(NCSe)_2(C_5H_5N)_2$ can be prepared and if this compound is isotopic to its Cd, Fe and Co analogs (see Section 4, *Thermoanalytical investigations*).

2. Structural commentary

The single-crystal structure determination proves that the title compound, $Mn(NCSe)_2(C_5H_5N)_4$, consists of discrete complexes. The asymmetric unit consists of one crystallographically independent Mn^{2+} cation that is located on a centre of inversion, as well as one selenocyanate anion and two pyridine ligands in general positions. The Mn^{2+} cation is octahedrally coordinated by four pyridine coligands and two terminally N-

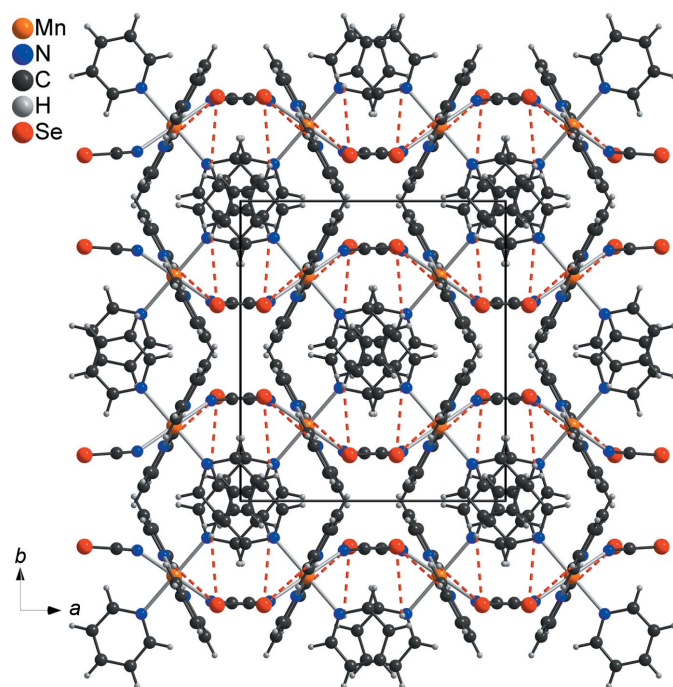


Figure 3
The crystal structure of the title compound, viewed along the crystallographic c -axis direction. C–H \cdots Se interactions are shown as red dashed lines.

bonded thiocyanate anions that are in *trans* positions (Fig. 2); the Mn–N bonds to the anions are notably shorter than the bonds to the pyridine molecules (Table 1) and the bond lengths are similar to those in the corresponding Fe and Co compounds. The *cis*-N–Mn–N angles deviate from the ideal octahedral values by up to 2°, which shows that the octahedra are slightly distorted.

It is noted that the title compound is isotopic to its Fe, Co, Zn and Cd analogues, with selenocyanate ligands, already described in the literature (Boeckmann & Näther, 2011; Boeckmann *et al.*, 2011, 2012). Moreover, the title compound is also isotopic to its thiocyanate analogs with Cu (Gary *et al.*, 2004; Li & Zhang, 2004), Cd (Qu *et al.*, 2004), Ni (Valach *et al.*, 1984; Wang *et al.*, 2006; Małeck *et al.*, 2010), Fe (Søtøfte & Rasmussen, 1967; Huang & Ogawa, 2006), Mn (Yang *et al.*, 2007; Małeck *et al.*, 2011), Co (Hartl & Brüdgam, 1980; Li *et al.*, 2007; Deng *et al.*, 2020), Mg (Lipkowski & Soldatov, 1993), Zn (Wu, 2004) and Co (Neumann *et al.*, 2019) (see Section 5, *Database survey*).

3. Supramolecular features

In the crystal structure of the title compound, the complexes are arranged into columns that propagate along the crystallographic c -axis direction (Fig. 3). As in the analogous compounds, there is no indication of aromatic π – π stacking

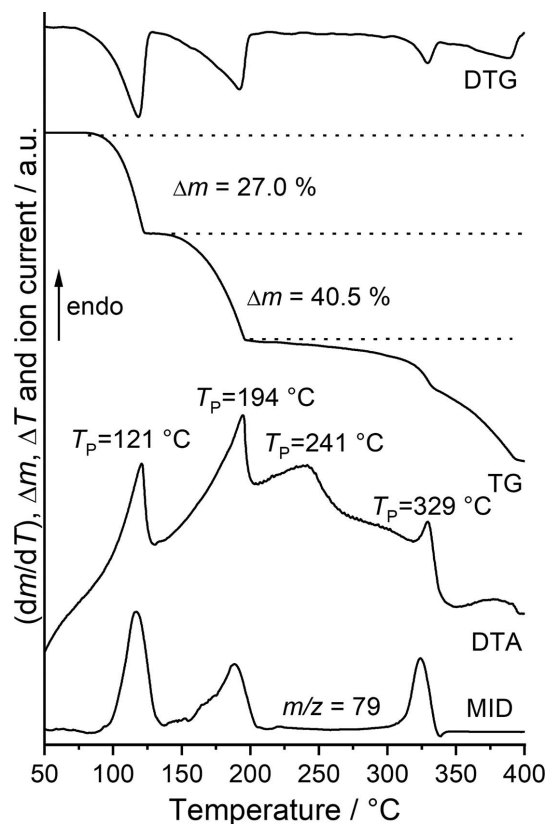


Figure 4
DTG, TG and DTA curves, and the MS trend scan curve for the title compound measured at 4 °C min⁻¹ in helium. The experimental mass loss is given in % and the peak temperatures are given in °C.

interactions. Within the structure, the $\text{Co}(\text{NCSe})_2$ units form corrugated layers that lie parallel to the ac plane (Fig. 3). Two $\text{C}-\text{H}\cdots\text{Se}$ contacts are observed with $\text{C}-\text{H}\cdots\text{Se}$ angles above 150° , which might indicate weak hydrogen-bonding interactions (Table 2). There are additional $\text{C}-\text{H}\cdots\text{Se}$ and $\text{C}-\text{H}\cdots\text{N}$ contacts, but from the distances and angles, it is concluded that they do not correspond to any significant interaction.

4. Thermoanalytical investigations

To investigate the thermal properties of the title compound, measurements using simultaneous differential thermoanalysis and thermogravimetry coupled to mass spectrometry (DTA–TG–MS) were performed. Upon heating, three mass losses are observed that are accompanied by endothermic events in the DTA curve (Fig. 4). The derivative thermogravimetric (DTG) curve shows that these events are reasonably resolved and from the MS trend scan curve it is obvious that in the first endothermic event, pyridine is removed. The experimental mass loss of 27.0% is in good agreement with that calculated for the removal of two pyridine ligands ($\Delta m_{\text{calc}} = -27.2\%$), whereas that in the second step is higher with a value of 40.5%, indicating that pyridine removal and the decomposition of $\text{Mn}(\text{NCSe})_2$ occur simultaneously. The fact that even in the third step pyridine might be removed indicates that the reaction is more complex, except that the signal at $m/z = 79$ corresponds to some fragment formed during decomposition.

However, to identify the product formed in the first mass loss this residue was isolated in a second TG measurement and investigated by IR and Raman spectroscopy, as well as PXRD. The CN stretching vibration of the selenocyanate anions is observed at 2099 cm^{-1} in the Raman and at 2090 cm^{-1} in the IR spectra, clearly proving that μ -1,3-bridging anionic ligands are present (Fig. S2 in the supporting information). The comparison of the experimental pattern with that calculated for $\text{Cd}(\text{NCSe})_2(\text{C}_5\text{H}_5\text{N})_2$, using single-crystal data retrieved from the literature, indicate that they are isotopic (Fig. S3). The pattern can easily be indexed, leading to a unit cell that is

comparable to that of the Cd, Fe and Co compounds. Finally, a Pawley fit of the experimental pattern using the crystallographic data of the cadmium compound (with Mn replacing Cd) as starting model was performed, which supports all these findings. The refined lattice parameters are shown together with the difference plot in Fig. 5. As expected, due to the smaller ionic radii, the unit-cell volume is smaller for the Mn compound compared to its Cd analogue [$1117.9(1)$ versus $1145.6(3)\text{ \AA}^3$] (Boeckmann *et al.*, 2011).

5. Database survey

A search in the Cambridge Structural Database (Version 5.43, last update November 2022; Groom *et al.*, 2016) using *ConQuest* (Bruno *et al.*, 2002) reveals that some selenocyanate compounds with pyridine coligands have been reported in the literature. These comprise discrete complexes with an octahedral coordination with the composition $M(\text{NCSe})_2(\text{C}_5\text{H}_5\text{N})_4$, with $M = \text{Fe}$ (CSD refcode CAQVEX; Boeckmann *et al.*, 2012), Co (ITISOU; Boeckmann & Näther, 2011), Zn (OWOHUE; Boeckmann *et al.*, 2011) and Cd (OWOJAM; Boeckmann *et al.*, 2011). The isotopic Ni compound $M(\text{NCSe})_2(\text{pyridine})_4$ was reported recently (Näther & Boeckmann, 2023). For the Co compound, mixed crystals with the composition $\text{Co}(\text{NCS})_x(\text{NCSe})_{2-x}(\text{C}_5\text{H}_5\text{N})_4$ have also been reported (TIXDOW and TIXDOW01; Neumann *et al.*, 2019).

As mentioned in the *Chemical context* section (Section 1) with pyridine, there also exist isotopic pyridine-deficient compounds with the composition $M(\text{NCSe})_2(\text{C}_5\text{H}_5\text{N})_2$, with $M = \text{Fe}$ (CAQVIB; Boeckmann *et al.*, 2012), Co (ITISUA; Boeckmann & Näther, 2011), Zn (OWOJEQ; Boeckmann *et al.*, 2011) and Cd (OWOHOY; Boeckmann *et al.*, 2011). In the first compounds, $M(\text{NCSe})_2$ chains are observed, whereas the Zn compound consists of discrete complexes.

One mixed-metal compound with the composition $\text{HgSr}(\text{NCSe})_4(\text{C}_5\text{H}_5\text{N})_6$ (CICLOP; Brodersen *et al.*, 1984), a dinuclear complex with the composition $[\text{Fe}(\text{NCS})_2]_2(\text{C}_5\text{H}_5\text{N})_2\text{-}[(3,5\text{-bis(pyridin-2-yl)pyrazolyl}]_2$ (FIZYEU; Sy *et al.*, 2014) and a complex with the composition $\text{Fe}(\text{NCSe})_2(\text{C}_5\text{H}_5\text{N})_2(2-$

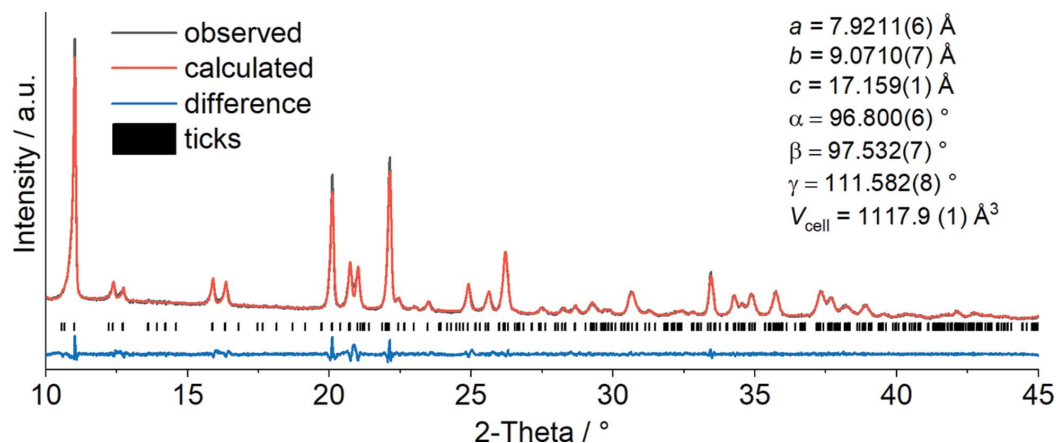


Figure 5
Pawley fit of $\text{Mn}(\text{NCSe})_2(\text{pyridine})_2$ obtained by TG measurements of the title compound $\text{Mn}(\text{NCSe})_2(\text{pyridine})_4$.

Table 3
Experimental details.

Crystal data	
Chemical formula	[Mn(NCSe) ₂ (C ₅ H ₅ N) ₂]
<i>M_r</i>	581.30
Crystal system, space group	Monoclinic, <i>C2/c</i>
Temperature (K)	170
<i>a</i> , <i>b</i> , <i>c</i> (Å)	12.5335 (9), 13.4331 (8), 15.1300 (12)
β (°)	108.608 (8)
<i>V</i> (Å ³)	2414.2 (3)
<i>Z</i>	4
Radiation type	Mo <i>K</i> α
μ (mm ⁻¹)	3.58
Crystal size (mm)	0.25 × 0.2 × 0.17
Data collection	
Diffractometer	Stoe IPDS2
Absorption correction	Numerical
<i>T_{min}</i> , <i>T_{max}</i>	0.332, 0.678
No. of measured, independent and observed [<i>I</i> > 2 σ (<i>I</i>)] reflections	8352, 2636, 2124
<i>R_{int}</i>	0.056
(<i>sin</i> θ / λ) _{max} (Å ⁻¹)	0.639
Refinement	
<i>R</i> [<i>F</i> ² > 2 σ (<i>F</i> ²)], <i>wR</i> (<i>F</i> ²), <i>S</i>	0.043, 0.088, 1.03
No. of reflections	2636
No. of parameters	142
H-atom treatment	H-atom parameters constrained
$\Delta\rho_{\max}$, $\Delta\rho_{\min}$ (e Å ⁻³)	0.56, -0.59

Computer programs: *X-AREA* (Stoe & Cie, 2008), *SHELXT2014* (Sheldrick, 2015a), *SHELXL2016* (Sheldrick, 2015b), *DIAMOND* (Brandenburg & Putz, 1999) and *publCIF* (Westrip, 2010).

methylidyridopyrido[3,2-*f*:2',3'-*h*]quinoxaline) pyridine solvate (TISWOI; Tao *et al.*, 2007) are also reported in the literature.

6. Synthesis and crystallization

MnCl₂·2H₂O, KNCS_e and pyridine were purchased from Alfa Aesar and used without any further purification.

6.1. Synthesis

0.25 mmol (49.7 mg) MnCl₂·2H₂O and 0.5 mmol (72.0 mg) KNCS_e were reacted with a mixture of 1.5 ml of pyridine and 1.5 ml of water. The mixture was stirred for 2 d at room temperature and the precipitate was filtered off, washed with very small amounts of water and dried in air. Single crystals were obtained under the same conditions but without stirring.

It is noted that even if a large excess of MnCl₂·2H₂O and KNCS_e was used in the synthesis, there are no hints for the formation of a pyridine-deficient compound with the composition Mn(NCSe)₂(pyridine)₂.

6.2. Experimental details

Single-crystal X-ray data were measured using an Image Plate Diffraction System (IPDS-2) from Stoe & Cie. Differential thermal analysis and thermogravimetric (DTA–TG–MS) measurements were performed in a dynamic helium atmosphere in Al₂O₃ crucibles using a Netzsch thermobalance with a skimmer coupling and a Balzer Quadrupol MS. The PXRD measurements were performed with a Stoe Transmis-

sion Powder Diffraction System (STADI P) with Cu *K* α ₁ radiation equipped with a linear position-sensitive MYTHEN 1K detector from Stoe & Cie. The IR data were measured using a Bruker Alpha-P ATR–IR spectrometer and the Raman spectra were measured with a Bruker Vertex 70 spectrometer.

7. Refinement

H atoms were positioned with idealized geometry (C–H = 0.95 Å) and refined with *U*_{iso}(H) = 1.2*U*_{eq}(C) using a riding model. Crystal data, data collection and structure refinement details are summarized in Table 3.

The Pawley fit for the diffraction pattern of Mn(NCSe)₂(C₅H₅N)₂ obtained by thermal decomposition was carried out using *TOPAS Academic* (Version 6.0; Coelho 2018). Initial lattice parameters were taken from Cd(NCSe)₂(C₅H₅N)₂: *R*_{wp} = 2.98%, *R*_{exp} = 2.08% and GOF = 1.44.

Acknowledgements

This work was supported by the state of Schleswig-Holstein.

References

- Boeckmann, J. & Näther, C. (2011). *Chem. Commun.* **47**, 7104–7106.
- Boeckmann, J., Reinert, T. & Näther, C. (2011). *Z. Anorg. Allg. Chem.* **637**, 940–946.
- Boeckmann, J., Wriedt, M. & Näther, C. (2012). *Chem. Eur. J.* **18**, 5284–5289.
- Brandenburg, K. & Putz, H. (1999). *DIAMOND*. Crystal Impact GbR, Bonn, Germany.
- Brodersen, K., Cygan, M. & Hummel, H. U. (1984). *Z. Naturforsch. B*, **39**, 2582–2585.
- Bruno, I. J., Cole, J. C., Edgington, P. R., Kessler, M., Macrae, C. F., McCabe, P., Pearson, J. & Taylor, R. (2002). *Acta Cryst.* **B58**, 389–397.
- Coelho, A. A. (2018). *J. Appl. Cryst.* **51**, 210–218.
- Deng, Y. F., Singh, M. K., Gan, D., Xiao, T., Wang, Y., Liu, S., Wang, Z., Ouyang, Z., Zhang, Y. Z. & Dunbar, K. R. (2020). *Inorg. Chem.* **59**, 7622–7630.
- Gary, J. B., Kautz, J. A., Klausmeyer, K. K. & Wong, C.-W. (2004). *Acta Cryst.* **E60**, m328–m329.
- Groom, C. R., Bruno, I. J., Lightfoot, M. P. & Ward, S. C. (2016). *Acta Cryst.* **B72**, 171–179.
- Gütlich, P., Garcia, Y. & Goodwin, H. A. (2000). *Chem. Soc. Rev.* **29**, 419–427.
- Hartl, H. & Brüdgam, I. (1980). *Acta Cryst.* **B36**, 162–165.
- Huang, W. & Ogawa, T. (2006). *J. Mol. Struct.* **785**, 21–26.
- Li, Y., Zhang, Z. X., Li, Q. S., Song, W. D., Li, K. C., Xu, J. Q., Miao, Y. L. & Pan, L. Y. (2007). *J. Coord. Chem.* **60**, 795–803.
- Li, Z.-X. & Zhang, X.-L. (2004). *Acta Cryst.* **E60**, m1597–m1598.
- Lipkowski, J. & Soldatov, D. (1993). *J. Coord. Chem.* **28**, 265–269.
- Małeck, J. G., Machura, B., Świtlicka, A., Groń, T. & Bałanda, M. (2011). *Polyhedron*, **30**, 746–753.
- Małeck, J. G., Świtlicka, A., Groń, T. & Bałanda, M. (2010). *Polyhedron*, **29**, 3198–3206.
- Mautner, F. A., Traber, M., Fischer, R. C., Torvisco, A., Reichmann, K., Speed, S., Vicente, R. & Massoud, S. S. (2018). *Polyhedron*, **154**, 436–442.
- Mekuimemba, C. D., Conan, F., Mota, A. J., Palacios, M. A., Colacio, E. & Triki, S. (2018). *Inorg. Chem.* **57**, 2184–2192.
- Näther, C. & Boeckmann, J. (2023). *Acta Cryst.* **E79**, 90–94.

- Neumann, T., Rams, M., Tomkowicz, Z., Jess, I. & Näther, C. (2019). *Chem. Commun.* **55**, 2652–2655.
- Palion-Gazda, J., Machura, B., Lloret, F. & Julve, M. (2015). *Cryst. Growth Des.* **15**, 2380–2388.
- Prananto, Y. P., Urbatsch, A., Moubaraki, B., Murray, K. S., Turner, D. R., Deacon, G. B. & Batten, S. R. (2017). *Aust. J. Chem.* **70**, 516–528.
- Qu, Y., Liu, Z.-D., Zhu, H.-L. & Tan, M.-Y. (2004). *Acta Cryst.* **E60**, m1013–m1014.
- Rams, M., Böhme, M., Kataev, V., Krupskaya, Y., Büchner, B., Plass, W., Neumann, T., Tomkowicz, Z. & Näther, C. (2020a). *Phys. Chem. Chem. Phys.* **19**, 24534–24544.
- Rams, M., Jochim, A., Böhme, M., Lohmiller, T., Ceglarska, M., Rams, M. M., Schnegg, A., Plass, W. & Näther, C. (2020b). *Chem. Eur. J.* **26**, 2837–2851.
- Senthil Kumar, K. & Ruben, M. (2017). *Coord. Chem. Rev.* **346**, 176–205.
- Sheldrick, G. M. (2015a). *Acta Cryst.* **A71**, 3–8.
- Sheldrick, G. M. (2015b). *Acta Cryst.* **C71**, 3–8.
- Shurdha, E., Moore, C. E., Rheingold, A. L., Lapidus, S. H., Stephens, P. W., Arif, A. M. & Miller, J. S. (2013). *Inorg. Chem.* **52**, 10583–10594.
- Søtofte, I. & Rasmussen, S. E. (1967). *Acta Chem. Scand.* **21**, 2028–2040.
- Stoe & Cie (2008). *X-Area, X-RED32 and X-SHAPE*. Stoe & Cie, Darmstadt, Germany.
- Sy, M., Varret, F., Boukheddaden, K., Bouchez, G., Marrot, S., Kawata, S. & Kaizaki, S. (2014). *Angew. Chem. Int. Ed.* **53**, 7539–7542.
- Tao, J. Q., Gu, Z. G., Wang, T. W., Yang, Q. F., Zuo, J. L. & You, X. Z. (2007). *Inorg. Chim. Acta*, **360**, 4125–4132.
- Valach, F., Sivý, P. & Koreň, B. (1984). *Acta Cryst.* **C40**, 957–959.
- Wang, C. F., Zhu, Z. Y., Zhou, X. G., Weng, L. H., Shen, Q. S. & Yan, Y. G. (2006). *Inorg. Chem. Commun.* **9**, 1326–1330.
- Werner, J., Rams, M., Tomkowicz, Z. & Näther, C. (2014). *Dalton Trans.* **43**, 17333–17342.
- Werner, J., Runčevski, T., Dinnebier, R., Ebbinghaus, S. G., Suckert, S. & Näther, C. (2015). *Eur. J. Inorg. Chem.* **2015**, 3236–3245.
- Westrip, S. P. (2010). *J. Appl. Cryst.* **43**, 920–925.
- Wöhlert, S., Ruschewitz, U. & Näther, C. (2012). *Cryst. Growth Des.* **12**, 2715–2718.
- Wriedt, M. & Näther, C. (2010). *Chem. Commun.* **46**, 4707–4709.
- Wu, C.-B. (2004). *Acta Cryst.* **E60**, m1490–m1491.
- Yang, H., Chen, Y., Li, D. & Wang, D. (2007). *Acta Cryst.* **E63**, m3186.

supporting information

Acta Cryst. (2023). E79, 482-487 [https://doi.org/10.1107/S2056989023003535]

Synthesis, crystal structure and thermal decomposition pathway of bis(isoselenocyanato- κ N)tetrakis(pyridine- κ N)manganese(II)

Christian Näther, Sebastian Mangelsen and Jan Boeckmann

Computing details

Data collection: *X-AREA* (Stoe & Cie, 2008); cell refinement: *X-AREA* (Stoe & Cie, 2008); data reduction: *X-AREA* (Stoe & Cie, 2008); program(s) used to solve structure: *SHELXT2014* (Sheldrick, 2015a); program(s) used to refine structure: *SHELXL2016* (Sheldrick, 2015b); molecular graphics: *DIAMOND* (Brandenburg & Putz, 1999); software used to prepare material for publication: *publCIF* (Westrip, 2010).

Bis(isoselenocyanato- κ N)tetrakis(pyridine- κ N)manganese(II)

Crystal data

[Mn(NCSe)₂(C₅H₅N)₂]
 $M_r = 581.30$
 Monoclinic, *C2/c*
 $a = 12.5335$ (9) Å
 $b = 13.4331$ (8) Å
 $c = 15.1300$ (12) Å
 $\beta = 108.608$ (8)°
 $V = 2414.2$ (3) Å³
 $Z = 4$

$F(000) = 1148$
 $D_x = 1.599$ Mg m⁻³
 Mo $K\alpha$ radiation, $\lambda = 0.71073$ Å
 Cell parameters from 8352 reflections
 $\theta = 2.4$ – 27.0 °
 $\mu = 3.58$ mm⁻¹
 $T = 170$ K
 Block, colorless
 $0.25 \times 0.2 \times 0.17$ mm

Data collection

Stoe IPDS-2
 diffractometer
 ω scans
 Absorption correction: numerical
 $T_{\min} = 0.332$, $T_{\max} = 0.678$
 8352 measured reflections
 2636 independent reflections

2124 reflections with $I > 2\sigma(I)$
 $R_{\text{int}} = 0.056$
 $\theta_{\max} = 27.0$ °, $\theta_{\min} = 2.4$ °
 $h = -16 \rightarrow 16$
 $k = -17 \rightarrow 16$
 $l = -18 \rightarrow 19$

Refinement

Refinement on F^2
 Least-squares matrix: full
 $R[F^2 > 2\sigma(F^2)] = 0.043$
 $wR(F^2) = 0.088$
 $S = 1.03$
 2636 reflections
 142 parameters
 0 restraints

Hydrogen site location: inferred from neighbouring sites
 H-atom parameters constrained
 $w = 1/[\sigma^2(F_o^2) + (0.0376P)^2 + 6.3344P]$
 where $P = (F_o^2 + 2F_c^2)/3$
 $(\Delta/\sigma)_{\max} = 0.001$
 $\Delta\rho_{\max} = 0.56$ e Å⁻³
 $\Delta\rho_{\min} = -0.59$ e Å⁻³

Special details

Geometry. All esds (except the esd in the dihedral angle between two l.s. planes) are estimated using the full covariance matrix. The cell esds are taken into account individually in the estimation of esds in distances, angles and torsion angles; correlations between esds in cell parameters are only used when they are defined by crystal symmetry. An approximate (isotropic) treatment of cell esds is used for estimating esds involving l.s. planes.

Fractional atomic coordinates and isotropic or equivalent isotropic displacement parameters (\AA^2)

	<i>x</i>	<i>y</i>	<i>z</i>	$U_{\text{iso}}^*/U_{\text{eq}}$
Mn1	0.750000	0.750000	0.500000	0.01953 (15)
N11	0.6262 (2)	0.6231 (2)	0.43418 (18)	0.0238 (6)
C11	0.6575 (3)	0.5279 (3)	0.4461 (2)	0.0318 (8)
H11	0.734043	0.513251	0.479058	0.038*
C12	0.5845 (3)	0.4496 (3)	0.4129 (3)	0.0406 (9)
H12	0.610081	0.382797	0.423720	0.049*
C13	0.4740 (3)	0.4701 (3)	0.3639 (3)	0.0454 (10)
H13	0.421823	0.417644	0.340179	0.054*
C14	0.4403 (3)	0.5677 (3)	0.3500 (3)	0.0480 (11)
H14	0.364597	0.583892	0.315879	0.058*
C15	0.5183 (3)	0.6422 (3)	0.3864 (3)	0.0347 (8)
H15	0.494330	0.709602	0.376995	0.042*
N21	0.7901 (2)	0.6823 (2)	0.64791 (18)	0.0222 (5)
C21	0.7567 (3)	0.7256 (3)	0.7149 (2)	0.0284 (7)
H21	0.717815	0.787259	0.701489	0.034*
C22	0.7765 (3)	0.6842 (3)	0.8025 (2)	0.0356 (8)
H22	0.752223	0.717571	0.848060	0.043*
C23	0.8319 (3)	0.5938 (3)	0.8230 (2)	0.0322 (8)
H23	0.846555	0.564051	0.882662	0.039*
C24	0.8654 (3)	0.5481 (3)	0.7544 (2)	0.0303 (7)
H24	0.902487	0.485410	0.765582	0.036*
C25	0.8441 (3)	0.5951 (3)	0.6690 (2)	0.0268 (7)
H25	0.869203	0.563732	0.622887	0.032*
Se1	0.41161 (3)	0.84748 (3)	0.58422 (3)	0.03339 (12)
C1	0.5323 (3)	0.8406 (2)	0.5460 (2)	0.0220 (6)
N1	0.6105 (2)	0.8349 (2)	0.5213 (2)	0.0291 (6)

Atomic displacement parameters (\AA^2)

	U^{11}	U^{22}	U^{33}	U^{12}	U^{13}	U^{23}
Mn1	0.0146 (3)	0.0198 (3)	0.0244 (3)	0.0001 (2)	0.0065 (2)	-0.0004 (3)
N11	0.0202 (12)	0.0227 (14)	0.0273 (14)	-0.0022 (10)	0.0058 (10)	-0.0023 (11)
C11	0.0340 (18)	0.0243 (18)	0.0366 (19)	-0.0002 (14)	0.0106 (15)	-0.0059 (14)
C12	0.054 (2)	0.0227 (18)	0.048 (2)	-0.0072 (18)	0.0202 (18)	-0.0072 (17)
C13	0.042 (2)	0.042 (2)	0.054 (2)	-0.0259 (19)	0.0172 (18)	-0.0170 (19)
C14	0.0282 (18)	0.047 (3)	0.059 (3)	-0.0131 (18)	-0.0003 (18)	-0.008 (2)
C15	0.0248 (16)	0.0302 (19)	0.043 (2)	-0.0020 (15)	0.0023 (15)	0.0006 (16)
N21	0.0169 (12)	0.0243 (14)	0.0243 (13)	-0.0015 (10)	0.0050 (10)	-0.0021 (10)
C21	0.0251 (15)	0.0305 (18)	0.0289 (17)	0.0007 (13)	0.0077 (13)	-0.0075 (13)

C22	0.0363 (19)	0.047 (2)	0.0261 (17)	-0.0025 (17)	0.0132 (14)	-0.0077 (15)
C23	0.0258 (16)	0.045 (2)	0.0255 (17)	-0.0024 (15)	0.0076 (13)	0.0036 (15)
C24	0.0242 (15)	0.0310 (18)	0.0338 (17)	0.0053 (14)	0.0066 (13)	0.0075 (15)
C25	0.0263 (16)	0.0279 (18)	0.0257 (16)	0.0040 (13)	0.0077 (13)	0.0007 (12)
Se1	0.0337 (2)	0.0309 (2)	0.0452 (2)	0.00150 (15)	0.02617 (16)	-0.00001 (16)
C1	0.0236 (14)	0.0158 (14)	0.0221 (15)	0.0007 (12)	0.0010 (12)	0.0007 (12)
N1	0.0211 (13)	0.0334 (16)	0.0351 (15)	0.0070 (12)	0.0120 (11)	0.0015 (12)

Geometric parameters (Å, °)

Mn1—N1 ⁱ	2.196 (3)	C14—H14	0.9500
Mn1—N1	2.196 (3)	C15—H15	0.9500
Mn1—N11 ⁱ	2.307 (3)	N21—C25	1.340 (4)
Mn1—N11	2.307 (3)	N21—C21	1.346 (4)
Mn1—N21	2.317 (3)	C21—C22	1.384 (5)
Mn1—N21 ⁱ	2.317 (3)	C21—H21	0.9500
N11—C11	1.332 (4)	C22—C23	1.384 (5)
N11—C15	1.339 (4)	C22—H22	0.9500
C11—C12	1.379 (5)	C23—C24	1.383 (5)
C11—H11	0.9500	C23—H23	0.9500
C12—C13	1.374 (6)	C24—C25	1.385 (5)
C12—H12	0.9500	C24—H24	0.9500
C13—C14	1.373 (6)	C25—H25	0.9500
C13—H13	0.9500	Se1—C1	1.786 (3)
C14—C15	1.384 (5)	C1—N1	1.157 (4)
N1 ⁱ —Mn1—N1	180.00 (15)	C13—C14—C15	119.1 (4)
N1 ⁱ —Mn1—N11 ⁱ	89.41 (10)	C13—C14—H14	120.4
N1—Mn1—N11 ⁱ	90.59 (10)	C15—C14—H14	120.4
N1 ⁱ —Mn1—N11	90.59 (10)	N11—C15—C14	122.6 (4)
N1—Mn1—N11	89.41 (10)	N11—C15—H15	118.7
N11 ⁱ —Mn1—N11	180.0	C14—C15—H15	118.7
N1 ⁱ —Mn1—N21	90.02 (10)	C25—N21—C21	117.0 (3)
N1—Mn1—N21	89.98 (10)	C25—N21—Mn1	120.7 (2)
N11 ⁱ —Mn1—N21	87.97 (9)	C21—N21—Mn1	122.3 (2)
N11—Mn1—N21	92.03 (9)	N21—C21—C22	122.9 (3)
N1 ⁱ —Mn1—N21 ⁱ	89.98 (10)	N21—C21—H21	118.5
N1—Mn1—N21 ⁱ	90.02 (10)	C22—C21—H21	118.5
N11 ⁱ —Mn1—N21 ⁱ	92.03 (9)	C21—C22—C23	119.4 (3)
N11—Mn1—N21 ⁱ	87.97 (9)	C21—C22—H22	120.3
N21—Mn1—N21 ⁱ	180.0	C23—C22—H22	120.3
C11—N11—C15	117.4 (3)	C24—C23—C22	118.2 (3)
C11—N11—Mn1	121.5 (2)	C24—C23—H23	120.9
C15—N11—Mn1	121.0 (2)	C22—C23—H23	120.9
N11—C11—C12	123.3 (3)	C23—C24—C25	118.9 (3)
N11—C11—H11	118.3	C23—C24—H24	120.5
C12—C11—H11	118.3	C25—C24—H24	120.5
C13—C12—C11	118.8 (4)	N21—C25—C24	123.6 (3)

C13—C12—H12	120.6	N21—C25—H25	118.2
C11—C12—H12	120.6	C24—C25—H25	118.2
C14—C13—C12	118.7 (3)	N1—C1—Se1	179.1 (3)
C14—C13—H13	120.6	C1—N1—Mn1	151.4 (3)
C12—C13—H13	120.6		

Symmetry code: (i) $-x+3/2, -y+3/2, -z+1$.

Hydrogen-bond geometry (Å, °)

<i>D</i> —H \cdots <i>A</i>	<i>D</i> —H	H \cdots <i>A</i>	<i>D</i> \cdots <i>A</i>	<i>D</i> —H \cdots <i>A</i>
C12—H12 \cdots Se1 ⁱⁱ	0.95	3.10	3.992 (4)	156
C22—H22 \cdots Se1 ⁱⁱⁱ	0.95	3.11	3.986 (4)	155
C25—H25 \cdots Se1 ^{iv}	0.95	3.04	3.757 (3)	133
C25—H25 \cdots N1 ⁱ	0.95	2.65	3.247 (4)	121

Symmetry codes: (i) $-x+3/2, -y+3/2, -z+1$; (ii) $-x+1, -y+1, -z+1$; (iii) $-x+1, y, -z+3/2$; (iv) $x+1/2, y-1/2, z$.